NJC

New Journal of Chemistry

A journal for new directions in chemistry

Accepted Manuscript

This article can be cited before page numbers have been issued, to do this please use: D. Ma, Y. Liu, B. Huang, L. Wang, X. Wang, Z. Sheng and F. Dong, *New J. Chem.*, 2019, DOI: 10.1039/C9NJ03461G.

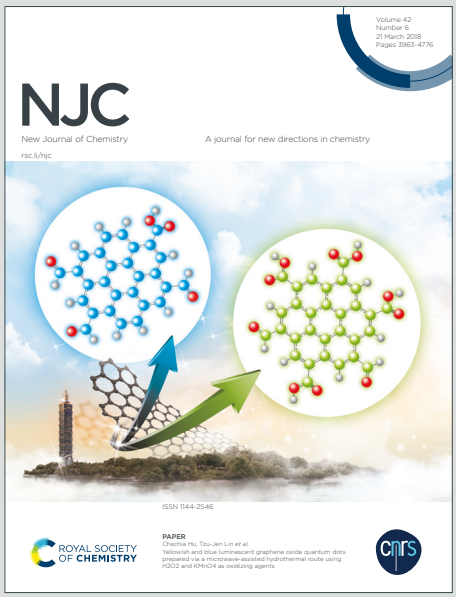

This is an Accepted Manuscript, which has been through the Royal Society of Chemistry peer review process and has been accepted for publication.

Accepted Manuscripts are published online shortly after acceptance, before technical editing, formatting and proof reading. Using this free service, authors can make their results available to the community, in citable form, before we publish the edited article. We will replace this Accepted Manuscript with the edited and formatted Advance Article as soon as it is available.

You can find more information about Accepted Manuscripts in the Information for Authors.

Please note that technical editing may introduce minor changes to the text and/or graphics, which may alter content. The journal's standard Terms & Conditions and the Ethical guidelines still apply. In no event shall the Royal Society of Chemistry be held responsible for any errors or omissions in this Accepted Manuscript or any consequences arising from the use of any information it contains.

View Article Online
DOI: 10.1039/C9NJ03461G

MnO_x-CeO_2 @ TiO_2 core-shell composites for low temperature SCR of NO_x

Dingren Ma,[ab] Liu Yang,[a] Bingjie Huang,[a] Liting Wang,[a] Xiao Wang,[a] Zhongyi Sheng*[ac] and Fan Dong[bd]

In this study, MnO_x-CeO_2 @ TiO_2 catalyst for NH_3-SCR of NO_x at low temperature was successfully prepared. TiO_2 was distributed on MnO_x-CeO_2 nanorod surface to form the core-shell structure. MnO_x-CeO_2 @ TiO_2 had excellent catalytic performance and SO_2 resistance. Characterization results indicated that excellent catalytic performance of MnO_x-CeO_2 @ TiO_2 could be mainly attributed to the large specific surface area, the presence of oxygen vacancies, the strong redox ability and the abundant acidic sites. Moreover, the catalytic active sites of MnO_x-CeO_2 @ TiO_2 could be protected from SO_2 poisoning due to the existence of the TiO_2 shell. MnO_x-CeO_2 @ TiO_2 was proved to be an excellent low temperature SCR catalyst.

[a] School of Environment, Nanjing Normal University, Nanjing 210023, Jiangsu, China
[b] Chongqing Key Laboratory of Catalysis and New Environmental Materials, College of Environment and Resources, Chongqing Technology and Business University, Chongqing 400067, China
[c] Suzhou Industrial Technology Research Institute of Zhejiang University, Suzhou 215163, Jiangsu, China
[d] Research Center for Environmental Science & Technology, Institute of Fundamental and Frontier Sciences, University of Electronic Science and Technology of China, Chengdu 611731, China

View Article Online
DOI: 10.1039/C9NJ03461G

1. Introduction

A large number of nitrogen oxides (NO_x) from coal-fired power plants have caused great harm to the environment and human beings.[1-3] Selective catalytic reduction (SCR) by urea or ammonia is one of the most effective technologies for the abatement of NO_x.[4-6] However, there are many defects in commercial SCR catalysts, such as narrow and high working temperature.[7-9] Therefore, the development of low temperature SCR catalysts is of great significance. MnO_x has excellent catalytic activity to remove NO_x at low temperature.[5] And CeO_2 has strong redox ability, oxygen storage capacity and acid-base property, which make it become a good catalyst.[10-17] The combination of MnO_x and CeO_2 exhibits superior catalytic performance. Therefore, MnO_x-CeO_2 catalysts are considered to be promising low temperature SCR catalysts. But the poor sulfur resistance of MnO_x-CeO_2 catalysts at low temperature still disturbs researchers.[10]

In order to improve the SO_2 tolerance of MnO_x-CeO_2 catalysts, researchers have used a variety of methods. Gao et al. found that MnO_x-CeO_2 modified by NiO and CoO_3 had larger surface area and more active sites, which improved catalytic activity and SO_2 resistance.[18] Chang et al. reported that Sn^{4+} doped MnO_x-CeO_2 also had excellent SO_2 resistance.[19, 20] Leng et al. investigated the Mn-Ce composite oxide catalyst supported on TiO_2 had excellent catalytic activity and sulfur resistance at low temperature.[21] Furthermore, core-shell nanostructures have been widely studied for special properties which can protect active components from migrating and sintering.[22] MnO_x @ TiO_2 core-shell catalyst not only showed excellent catalytic activity at low temperature, but also had good SO_2 resistance.[23] Chen et al. found that

hierarchical Fe-ZSM-5 @ CeO_2 catalyst constructed a fast-SCR environment and exhibited favorable water resistance.[24] Moreover, mesoporous TiO_2 @ Fe_2O_3 core-shell composites were prepared to improve the low temperature SO_2-tolerant.[25]

Herein, in order to take advantages of core-shell structure, MnO_x-CeO_2 nanorods were first prepared by a template method. Then the surface of MnO_x-CeO_2 nanorods was covered by TiO_2 particles and core-shell structure catalyst marked as MnO_x-CeO_2 @ TiO_2 was successfully prepared. The effects of MnO_x-CeO_2 @ TiO_2 with unique core-shell structure on catalytic activity and SO_2 resistance at low temperature were investigated. The MnO_x-CeO_2 @ TiO_2 catalyst may act as a potential candidate for the NH_3-SCR reaction at low temperature due to its excellent performance.

2. Experimental

2.1. Catalyst preparation

2.1.1. MnO_x-CeO_2 @ TiO_2

MnO_x-CeO_2 @ TiO_2 was prepared by a three-step method. $Ce(OH)CO_3$ templates were first prepared and then MnO_x-CeO_2 nanorods were prepared by an oxidation-reduction process. Finally, MnO_x-CeO_2 @ TiO_2 was prepared by a versatile kinetics-controlled coating method.[26]

In an oil bath at 80 ^oC, 0.02 mol $Ce(NO_3)_3$ $6H_2O$ and 0.12 mol urea were sequentially added to 400 mL deionized water and stirred for 24 h. The solution was centrifuged to obtain white precipitate, and the precipitate was washed with distilled water to remove excess impurities until the pH of supernatant was about 7.

View Article Online
DOI: 10.1039/C9NJ03461G

$Ce(OH)CO_3$ was obtained after drying at 60 ^oC for 6 hours in an oven.

20 mL $Mn(NO_3)_2$ (0.025M) was first prepared and 1.25g $Ce(OH)CO_3$ was added to the solution under magnetic stirring. The mixture was further stirred ceaselessly for 30 min and then kept still for 6 days. The sediment was sequentially washed with 1M HNO_3 and deionized water. Finally, MnO_x-CeO_2 composite was acquired by drying at 80 ^oC for 12 hours.

0.26 g MnO_x-CeO_2 was distributed uniformly in 100 mL ethanol. 0.3 mL ammonia was added to the above solution under ultrasonic processing for 30 minutes. Then 0.75 mL tetrabutyl titanate was added to the mixture under magnetic stirring for 24 hours at 45 ^oC. The precipitate was rinsed three times with deionized water. At last, the resulting powder was dried at 80 ^oC for 12 hours and calcined in air at 500 ^oC for 2 hours. The sample was denoted as MnO_x-CeO_2 @ TiO_2.

2.1.2. MnO_x-CeO_2 / TiO_2

The corresponding MnO_x-CeO_2 / TiO_2 sample was prepared by a one-step hydrothermal method. 0.03 mol $Ce(NO_3)_3$ $6H_2O$ was dissolved in 100 mL $Mn(NO_3)_2$ (0.025M) solution at room temperature. Then 7.5 mL ammonia and 19 mL tetrabutyl titanate were added to the above solution. The mixture was further stirred ceaselessly for 30 minutes and then sealed in a Teflon-lined stainless steel autoclave at 130 ^oC for 12 hours. The sediment was washed with deionized water and dried at 80 ^oC for 12 hours. Finally, the powder was calcined in air at 500 ^oC for 2 hours, which was defined as MnO_x-CeO_2 / TiO_2.

View Article Online
DOI: 10.1039/C9NJ03461G

2.2. Catalysts characterization

X-ray diffraction (XRD) with Cu-Kα radiation was used for testing the crystalline structures of samples. The morphology and structure of samples were analyzed by transmission electron microscopy (TEM). The pore distribution and surface area were calculated by Brunauer-Emmett-Teller (BET) equation using Micromeritics ASSP 2020 equipment at 77K by N_2 physisorption. The Raman spectra of samples were collected by Raman spectrometer (Renishaw RM 2000) with a laser at 514 nm. X-ray photoelectron spectroscopy (XPS) was used for analyzing the surface atomic states of samples. NH_3 temperature-programmed desorption (NH_3-TPD) was performed on the TP 5080 automatic multi-purpose adsorption instrument (Xianquan, China). The samples (150 mg) were pretreated at 300 ℃ in a flow of N_2 (30 mL·min^{-1}) for 0.5 h and cooled to 100 ℃ under N_2 flow. Then the samples were saturated with NH_3 at 100 ℃ for 1 h, followed by N_2 purging for 0.5 h until there was no NH_3 signal detected. Finally, the temperature was raised to 800 ℃ in N_2 at a ramping rate of 10 ℃·min^{-1}. And the results of H_2 temperature-programmed reduction (H_2-TPR) were recorded on the same instrument.

2.3 Activity measurements

NH_3-SCR activity measurements were performed in a temperature controlled fixed-bed. In the experiment, air flow rate was 1600 mL·min^{-1} and airspeed was 24000 h^{-1}. The concentration of reaction gases were as follows: 500 ppm NO, 500 ppm NH_3 and 5% O_2, (200 ppm SO_2) and N_2 as the balance gas. The inlet and outlet

concentrations of SO_2, O_2, NO_2 and NO were measured by a flue gas analyzer (MRU Vario Plus, Germany). And the outlet concentration of N_2O was monitored by another gas analyzer (G200). NO_x conversion and N_2 selectivity of samples were calculated as follows respectively:

$$O_x \text{ conversion } (\%) = \frac{C^{in}_{NO_x} - C^{out}_{NO_x}}{C^{in}_{NO_x}} \times 100$$

$$N_2 \text{ selectivity } (\%) = \left(1 - \frac{2C^{out}_{N_2O}}{C^{in}_{NO_x} + C^{in}_{NH_3} - C^{out}_{NO_2} - C^{out}_{NO} - C^{out}_{NH_3}}\right) \times 100$$

where $NO_x = NO + NO_2 + 2N_2O$.

3. Results and discussion

3.1 XRD patterns

The phase compositions of MnO_x-CeO_2 / TiO_2 and MnO_x-CeO_2 @ TiO_2 were determined by XRD. Fig. 1 shows the XRD patterns of MnO_x-CeO_2 / TiO_2 and MnO_x-CeO_2 @ TiO_2. Characteristic peaks of CeO_2 (JCPDS card No. 81-0792) and TiO_2 (JCPDS card No. 89-4921) can be found in both samples. There are no obvious peaks of MnO_x, indicating that MnO_x are highly dispersed on the samples. And highly dispersed active components would contribute to increase the catalytic activity of catalysts.[27] Compared with MnO_x-CeO_2 / TiO_2, the characteristic peaks of CeO_2 in MnO_x-CeO_2 @ TiO_2 are significantly reduced. The reasons for this are that CeO_2 and MnO_x are well integrated and MnO_x-CeO_2 is wrapped by TiO_2, resulting in a decrease

View Article Online
DOI: 10.1039/C9NJ03461G

of the strength of the CeO_2 diffraction peak.[28]

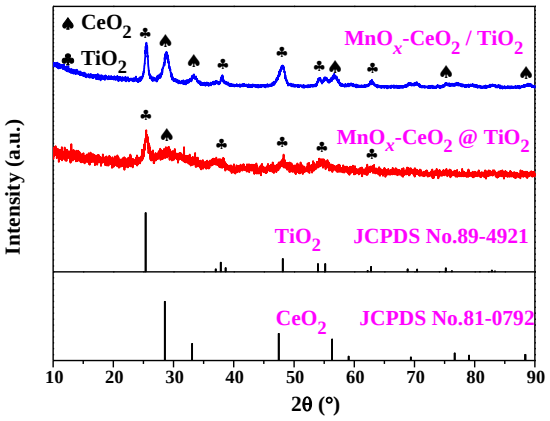

Fig. 1 XRD patterns of MnO_x-CeO_2 / TiO_2 and MnO_x-CeO_2 @ TiO_2

3.2 TEM images

The morphologies and structures of the samples were observed by TEM. As shown in Fig. 2a, the nanoparticles have a large spacing from each other, indicating that MnO_x-CeO_2 / TiO_2 has no special core-shell structure. In Fig. 2b, Mn-Ce nanorods are wrapped by TiO_2 nanoparticles to form the core-shell structure. The formation of the core-shell structure is consistent with the conclusions obtained in XRD. Fig. 2c shows a HRTEM image of MnO_x-CeO_2 @ TiO_2. It can be seen that the nanorod structure is very clear and some nanoparticles are attached to the nanorod. The distinct lattice fringes are measured to be about 0.306 nm and 0.292 nm, which matche well with the (311) crystal plane of CeO_2 and the (105) crystal plane of TiO_2, respectively. Moreover, Fig. 2d shows that MnO_x-CeO_2 @ TiO_2 is polycrystalline.[29]

View Article Online
DOI: 10.1039/C9NJ03461G

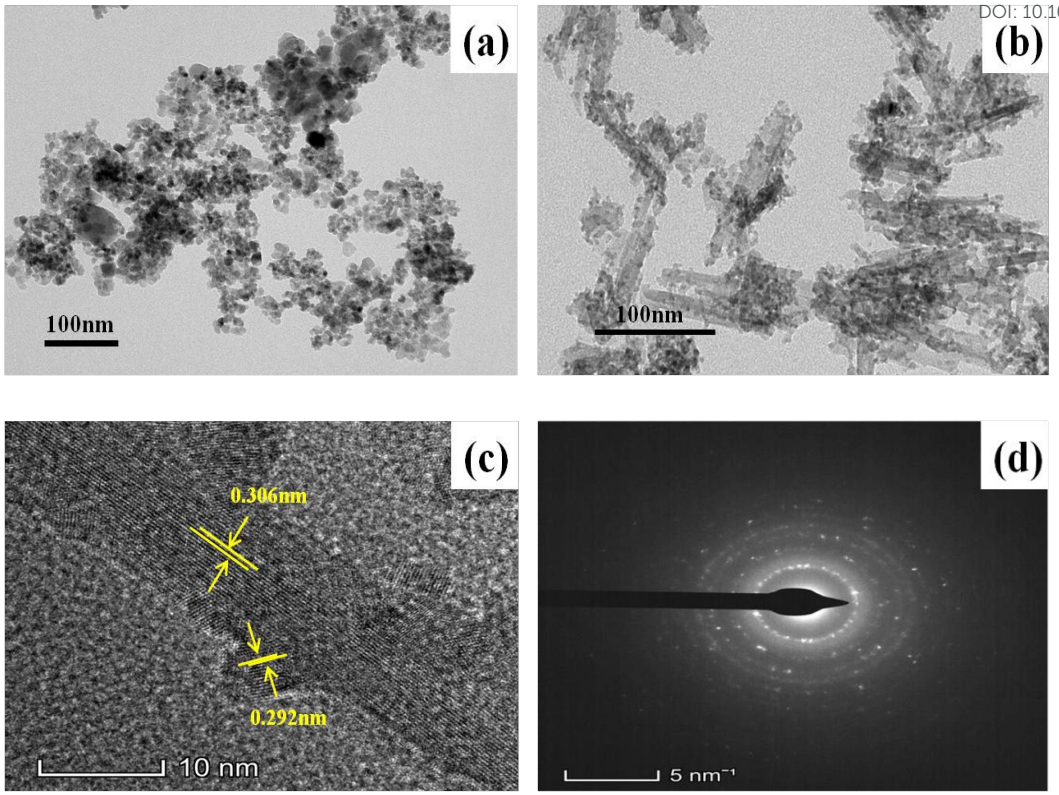

Fig. 2 TEM images of MnO_x-CeO_2 / TiO_2 (a) and MnO_x-CeO_2 @ TiO_2 (b), HRTEM image and SAED pattern of MnO_x-CeO_2 @ TiO_2 (c, d).

3.3 Raman Patterns

Raman spectroscopy was performed to further analyze the crystal structures of samples. As shown in Fig. 3, MnO_x-CeO_2 / TiO_2 presents bands located at 142, 460 and 577 cm^{-1}. Band at 142 cm^{-1} coincides with anatase TiO_2,[30, 31] characteristic band at 460 cm^{-1} belongs to pure CeO_2 [32]and band at 577 cm^{-1} can be assigned to α-MnO_2.[33] Obviously, the α-MnO_2 characteristic band of MnO_x-CeO_2 @ TiO_2 shifts to higher wavenumber compared with MnO_x-CeO_2 / TiO_2, which is the result of the action of oxygen vacancies.[34] The presence of oxygen vacancies facilitates the destruction of N-O bonds and thus increases catalytic activity.[32] The CeO_2 band of

View Article Online
DOI: 10.1039/C9NJ03461G

MnO_x-CeO_2 @ TiO_2 exhibits a red shift compared with MnO_x-CeO_2 / TiO_2, which is related to the formation of Mn-Ce nanorods. Due to the interaction of TiO_2 and Mn-Ce nanorods, the band of TiO_2 shifts to lower wavenumber.[34]

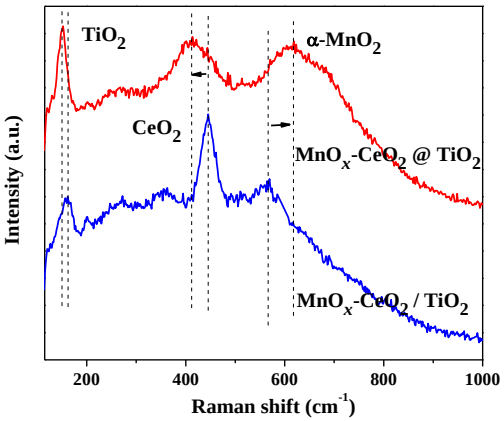

Fig. 3 Raman spectra of MnO_x-CeO_2 / TiO_2 and MnO_x-CeO_2 @ TiO_2

3.4 BET analysis

The pore size distributions and BET surface areas of the different samples are shown in Table 1. And the N_2 adsorption-desorption isotherms are displayed in Fig. 4. Both curves in Fig. 4 have significant hysteresis loops in the P/P_0 range of 0.6 to 1 and are assigned to the type IV according to IUPAC classification, indicating that the samples have large amounts of mesoporous.[35] Rich mesoporous structure would provide channels for the reaction gases to enter into the inner surface of catalyst to improve the catalytic performance.[36] As shown in Table 1, the specific surface area of MnO_x-CeO_2 @ TiO_2 is larger than MnO_x-CeO_2 / TiO_2, which is conducive to the improvement of catalytic performance. The large specific surface area of MnO_x-CeO_2 @ TiO_2 may be due to the formation of hollow nanorods.[37]

View Article Online
DOI: 10.1039/C9NJ03461G

Table 1 BET surface areas and pore parameters of catalysts

	S_{BET}（m^2/g）	Pore volume（10^{-2} cm^3/g）	Average pore diameter（nm）
MnO_x-CeO_2/TiO_2	71.71	0.25	13.72
MnO_x-CeO_2@TiO_2	110.65	0.37	13.26

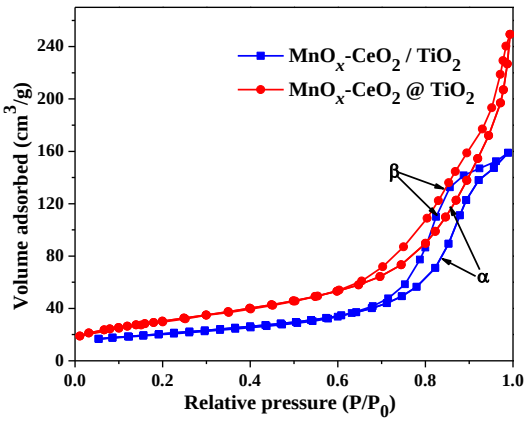

Fig. 4 N_2 adsorption-desorption isotherms of MnO_x-CeO_2 / TiO_2 and MnO_x-CeO_2 @ TiO_2

3.5 XPS

The XPS spectra of Mn, Ce, Ti and O are shown in Fig. 5 and relative atomic concentrations are listed in Table 2. In Fig. 5a, Mn $2p_{3/2}$ spectra can be divided into two characteristic peaks which correspond to Mn^{3+} at 640.90eV and Mn^{4+} at 642.80eV respectively.[38] Mn $2p_{1/2}$ peak appear at 652.80 eV, which is related to Mn^{4+}.[39] As shown in Table 2, the content of Mn is higher on the surface of MnO_x-CeO_2 / TiO_2 than that of MnO_x-CeO_2 @ TiO_2, which is due to the formation of nanorod and core-shell structure. Moreover, the NO conversions decreased in the order of MnO_2 > Mn_5O_8 > Mn_2O_3 > Mn_3O_4 in low-temperature SCR reaction.[10] The

View Article Online
DOI: 10.1039/C9NJ03461G

proportion of Mn^{4+} in MnO_x-CeO_2 @ TiO_2 is higher than MnO_x-CeO_2 / TiO_2, indicating that MnO_x-CeO_2 @ TiO_2 has excellent catalytic activity.

The XPS results of Ce 3d spectra are shown in Fig. 5b. It can be seen that Ce 3d spectra can be divided into eight different peaks. These eight peaks can be divided into two kinds, one is the $3d_{3/2}$ corresponding peaks labeled as u and the other is the $3d_{5/2}$ corresponding peaks labeled as v. The peaks denoted as u, u'', u''' and v, v'', v''' are assigned to Ce^{4+} while u' and v' are assigned to Ce^{3+}.[40] As shown in Table 2, Ce mainly exists in the form of Ce^{4+} in samples. Interestingly, the production of Ce^{3+} is related to the formation of oxygen vacancies.[32] According to the Raman results, the oxygen vacancies in MnO_x-CeO_2 @ TiO_2 favor the formation of Ce^{3+}, which is consistent with the higher Ce^{3+} content of MnO_x-CeO_2 @ TiO_2.

Fig. 5c shows the XPS results of Ti 2p. The peak at around 459.5 eV corresponds to TiO_2.[41] Ti exists in the form of Ti^{4+} on the surface of MnO_x-CeO_2 / TiO_2 and MnO_x-CeO_2 @ TiO_2. The content of Ti in MnO_x-CeO_2 @ TiO_2 is higher than MnO_x-CeO_2 / TiO_2. This result indicates that MnO_x-CeO_2 is wrapped by TiO_2, which consistent with the results of TEM.

In Fig. 5d, two distinct peaks appear. One is chemisorbed oxygen (O_α) located at 530.9eV and the other is lattice oxygen (O_β) located at 528.8 eV.[1] The higher the content of O_α, the more conducive to the SCR catalytic reaction.[6] Table 2 shows that the ratio of O_α in MnO_x-CeO_2 @ TiO_2 is higher than MnO_x-CeO_2 / TiO_2, which can promote the oxidation of NO to NO_2, thereby increasing the catalytic activity.[42]

View Article Online
DOI: 10.1039/C9NJ03461G

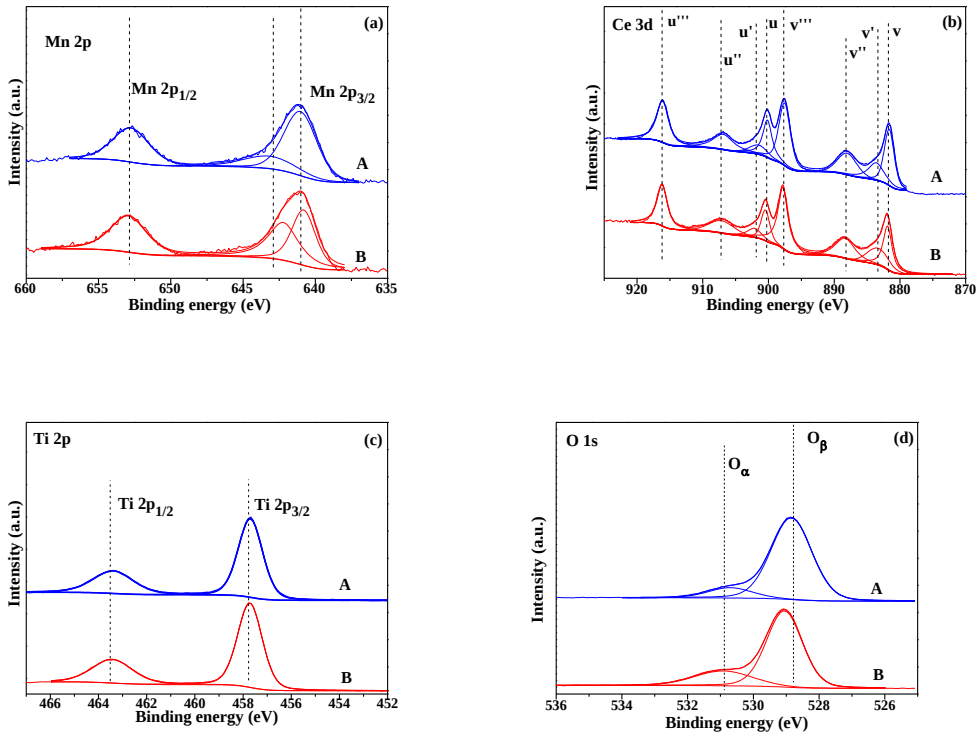

Fig. 5 XPS spectra of catalyst surface elements Mn 2p (a), Ce 3d (b), Ti 2p (c) and O 1s (d)

（A: MnO_x-CeO_2 / TiO_2; B: MnO_x-CeO_2 @ TiO_2）

Table 2 Atomic surface composition of the catalysts as determined by XPS

Samples	Atomic composition (%)				Relative atomic ratio (%)					
					Mn		O		Ce	
	Mn	Ti	O	Ce	Mn^{4+}	Mn^{3+}	O_α	O_β	Ce^{4+}	Ce^{3+}
MnO_x-CeO_2/TiO_2	4.16	14	53.75	7.53	48.9	51.1	12.26	87.74	86.22	13.78
MnO_x-CeO_2@TiO_2	4.01	15.84	56.6	5.32	67.42	32.58	23.42	76.58	85.61	14.39

3.6 NH_3-TPD

View Article Online
DOI: 10.1039/C9NJ03461G

Obviously, the surface acidity of samples play an important role in the NH_3-SCR reaction.[4] In order to explore the surface acidity of samples, NH_3-TPD results are shown in Fig. 6. There is a broad peak at 200 ℃ for the samples, which is formed by the desorption of adsorbed NH_3 on medium acid and weak acid sites.[34] The peak located in the temperature range from 200 to 500 ℃ is attributed to the Brønsted acid sites.[43] It can be seen that the peak area of MnO_x-CeO_2 @ TiO_2 is larger than MnO_x-CeO_2 / TiO_2, especially in the Brønsted acid position, indicating that MnO_x-CeO_2 @ TiO_2 has more acidic sites.[44] Obviously, MnO_x-CeO_2 @ TiO_2 possesses excellent NH_3 adsorption capacity, which is conducive to the NH_3-SCR reaction.

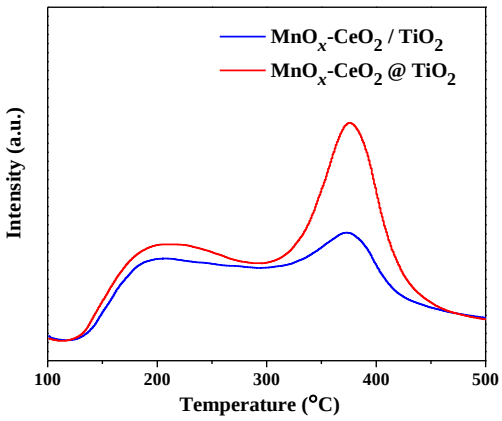

Fig. 6 NH_3-TPD pattern of MnO_x-CeO_2 / TiO_2 and MnO_x-CeO_2 @ TiO_2

3.7 H_2-TPR

In order to examine the reducibility of the samples, H_2-TPR measurements were performed. As shown in Fig. 7, MnO_x-CeO_2 @ TiO_2 has two peaks located at 241 ℃ and 345 ℃ respectively. The peak at 241 ℃ is due to the reduction of MnO_2 to Mn_3O_4.

View Article Online
DOI: 10.1039/C9NJ03461G

And the peak at 345 ℃ corresponds to the reduction of Mn_3O_4 to MnO when the surface capping oxygen of CeO_2 is reduced.[45] Furthermore, MnO_x-CeO_2 / TiO_2 has two peaks similar to MnO_x-CeO_2 @ TiO_2. But the two peaks shift to higher temperature, indicating the oxidation performance of MnO_x-CeO_2 / TiO_2 is weaker than MnO_x-CeO_2 @ TiO_2.[46]

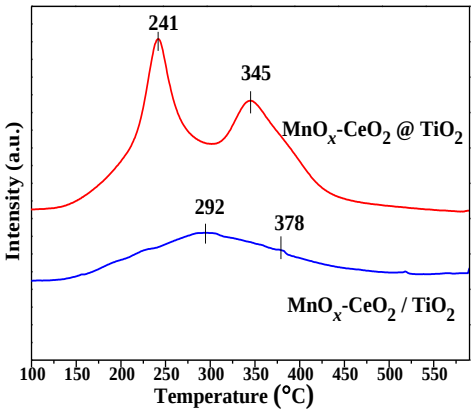

Fig. 7 H_2-TPR patterns of MnO_x-CeO_2 / TiO_2 and MnO_x-CeO_2 @ TiO_2

3.8 Catalytic Performance

The catalytic performance of prepared samples towards NO removal was evaluated. As shown in Fig. 8a, MnO_x-CeO_2 / TiO_2 and MnO_x-CeO_2 @ TiO_2 exhibit high catalytic activity at low temperature. The NO_x conversion of MnO_x-CeO_2 @ TiO_2 reaches around 100% at 140 ^oC. And the catalytic activity of MnO_x-CeO_2 / TiO_2 is lower than MnO_x-CeO_2 @ TiO_2, which is consistent with the conclusions obtained before. N_2 selectivity is a crucial role in evaluating the catalytic activity of SCR catalyst. In Fig. 8b, the N_2 selectivity of MnO_x-CeO_2 / TiO_2 gradually decreases with the increase of temperature. These results can be attributed to the formation of N_2O

View Article Online
DOI: 10.1039/C9NJ03461G

under high load and partial oxidation of NH_3 at elevated temperatures.[47] And Mn-based catalysts, due to their oxidative power, promote the formation of undesired products (N_2O and NO_2).[48] In addition, the N_2 selectivity of MnO_x-CeO_2 @ TiO_2 remains above 95% from 40 to 200 ^oC. As shown in the Raman spectra, a synergistic interface effect exists between MnO_x-CeO_2 (core) and TiO_2 (shell), which facilitates NH_3-SCR activities of MnO_x-CeO_2 @ TiO_2 catalysts and N_2 selectivity.[49] The stability of MnO_x-CeO_2 @ TiO_2 at 160 ^oC is shown in Fig. 8c. And the NO_x conversion of MnO_x-CeO_2 @ TiO_2 remains unchanged in the whole test, which is due to the formation of the core-shell structure.[50] Core-shell nanostructures protect active components from migrating and reuniting. It can be concluded that MnO_x-CeO_2 @ TiO_2 has high N_2 selectivity, good stability and high SCR activity, which is closely related to its special core-shell structure.

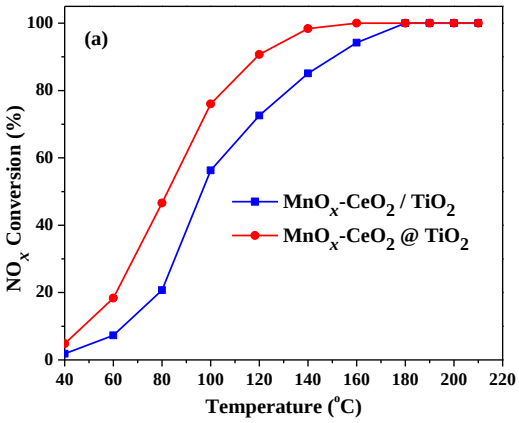

View Article Online
DOI: 10.1039/C9NJ03461G

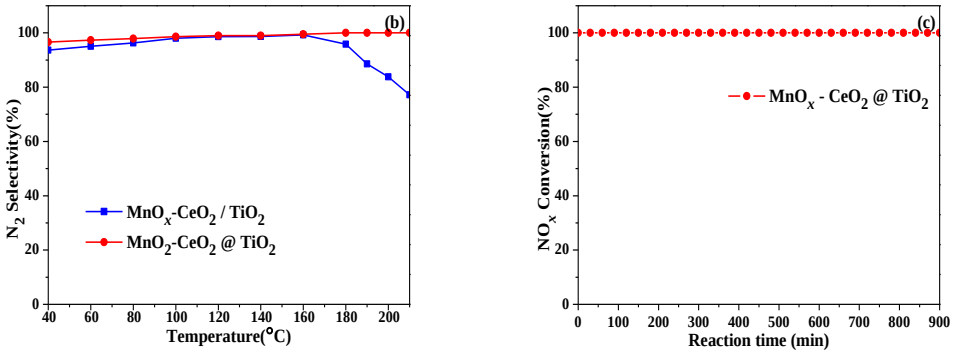

Fig. 8 Catalytic activity (a) and N_2 selectivity (b) for different samples and stability of MnO_x-CeO_2 @ TiO_2 catalyst at 160 ℃ (c)

3.9 Influence of SO_2

High SO_2 durability is usually required for the potential low-temperature NH_3-SCR catalysts. 200ppm SO_2 was added into the system on the basis of the catalytic activity test. The catalytic activity of MnO_x-CeO_2 / TiO_2 and MnO_x-CeO_2 @ TiO_2 are shown in Fig. 9.

After 200ppm SO_2 was introduced into flue gas system for 3.5 hours, catalytic activity of MnO_x-CeO_2 / TiO_2 and MnO_x-CeO_2 @ TiO_2 decreased from 100% to 47% and 70% respectively, verifying that SO_2 had a poisoning effect on SCR activity at low temperature. Catalytic activity of MnO_x-CeO_2 / TiO_2 could not recover after the removal of SO_2, indicating that SO_2 caused irreparable damage to MnO_x-CeO_2 / TiO_2. Compared with MnO_x-CeO_2 / TiO_2, the activity of MnO_x-CeO_2 @ TiO_2 restored to around 85% after turning off the SO_2.

View Article Online
DOI: 10.1039/C9NJ03461G

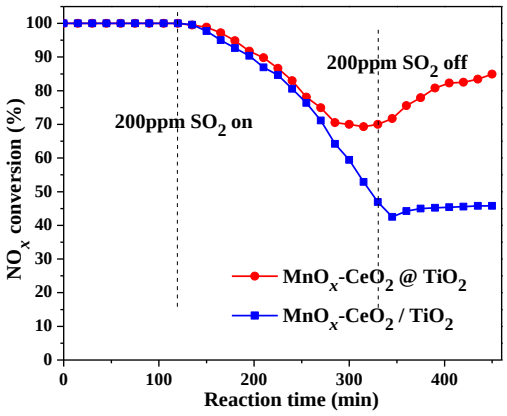

Fig. 9 SO_2 tolerance of MnO_x-CeO_2 / TiO_2 and MnO_x-CeO_2 @ TiO_2 at 180 ^oC

According to literatures, the formation and deposition of ammonium sulfates which clog the pore channels and the competitive adsorption between NO and SO_2 partially contribute to the deactivation of catalyst. And the main cause of catalyst deactivation is the sulfation of the active center atoms.[51] Gao et al. reported that MnO_x-based catalysts have poor resistance to SO_2.[52] MnO_x-based catalysts can easily react with SO_2 to generate a large amount of sulfate, resulting in a decrease of the amount of the active component of Mn^{4+}. When SO_2 was added into system, MnO_x-CeO_2 @ TiO_2 had higher catalytic activity than MnO_x-CeO_2 / TiO_2. As shown in Fig.2a, the active components of MnO_x-CeO_2 / TiO_2 were completely exposed. The surface of MnO_x-CeO_2 / TiO_2 was covered with ammonium sulfate to prevent the adsorption of the reaction gas. Moreover, the active components of MnO_x-CeO_2 / TiO_2 reacted with SO_2 to generate a large amount of sulfate that did not contribute to NO degradation, which was the reason why the catalytic activity of MnO_x-CeO_2 / TiO_2 could not recover after the removal of SO_2. Compared with MnO_x-CeO_2 / TiO_2,

View Article Online
DOI: 10.1039/C9NJ03461G

the special core-shell structure in MnO_x-CeO_2 @ TiO_2 caused ammonium sulfate to deposit on the outer shell, which reduced the blockage of the catalyst channel by ammonium sulfate. Interestingly, the active center is not easily exposed to SO_2 due to the presence of the TiO_2 outer shell.[32] MnO_x-CeO_2 @ TiO_2 still had a large number of active centers after SO_2 was added into the system for several hours. So MnO_x-CeO_2 @ TiO_2 had higher catalytic activity than MnO_x-CeO_2 / TiO_2. And the decomposition of ammonium sulfate and the disappearance of competitive adsorption of SO_2 were probably responsible for the recovery of MnO_x-CeO_2 @ TiO_2 activity after the removal of SO_2.

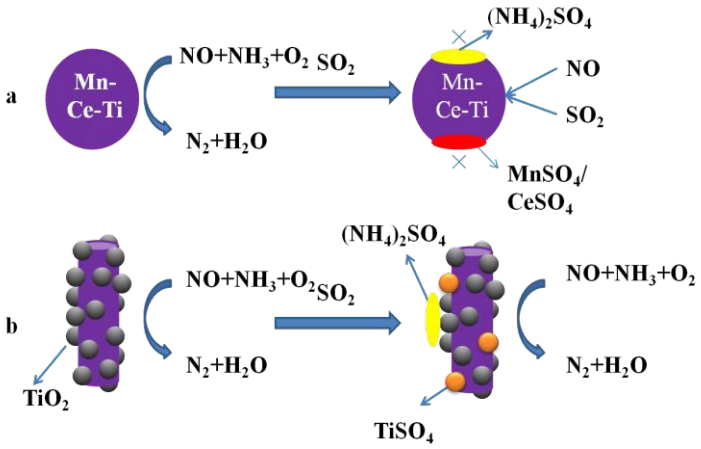

Fig. 10 The SO_2 deactivation mechanism over different catalysts. (a) MnO_x-CeO_2 / TiO_2; (b) MnO_x-CeO_2 @ TiO_2.

4. Conclusion

In summary, core-shell structure MnO_x-CeO_2 @ TiO_2 was successfully fabricated as high-performance de-NO_x catalyst. Compared with MnO_x-CeO_2 / TiO_2, MnO_x-CeO_2 @ TiO_2 has larger specific surface area and pore volume, which make

View Article Online
DOI: 10.1039/C9NJ03461G

the catalyst have more active sites and channels for the reaction gas to fully contact the active sites. Moreover, more oxygen vacancies and acidic sites in MnO_x-CeO_2 @ TiO_2 make NO more susceptible to oxidation. Obviously, The TiO_2 shell not only does not inhibit the catalytic activity of MnO_x-CeO_2 @ TiO_2, but improves the physicochemical properties of the catalysts. The superior SO_2 tolerance could be attributed to the unique core-shell structure lowers the possibility of surface active sites poisoned by SO_2 and meanwhile prevents the formation of ammonium sulfate species from covering the active sites. The MnO_x-CeO_2 @ TiO_2 catalyst could serve as a promising candidate for the NH_3-SCR catalyst at low temperature.

Conflicts of interest

There are no conflicts to declare.

Acknowledgments

This work was funded by the National Natural Science Foundation of China (no. 41877469 and 51508281).

Notes and references

1. J. Yu, Z. C. Si, X. K. Li, L. Chen, X. D. Wu and D. Weng, *Catal. Today*, 2016, **267**, 47-55.
2. A. Beretta, A. Lanza, L. Lietti, S. A. Clave, J. Collier and M. Nash, *Chem. Eng. J.*, 2019, **359**, 88-98.
3. H. Hu, S. X. Cai, H. R. Li, L. Huang, L. Y. Shi and D. S. Zhang, *Acs Catal.*, 2015, **5**, 6069-6077.
4. X. L. Li and Y. H. Li, *J. Mol. Catal. a-Chem.*, 2014, **386**, 69-77.
5. Y. R. Yang, M. H. Wang, Z. L. Tao, Q. Liu, Z. Y. Fei, X. Chen, Z. X. Zhang, J.

H. Tang, M. F. Cui and X. Qiao, *Catal. Sci. & Technol.*, 2018, **8**, 6396-6406.

6. Z. M. Liu, Y. Li, T. L. Zhu, H. Su and J. Z. Zhu, *Ind. & Eng. Chem. Res.*, 2014, **53**, 12964-12970.
7. W. Y. Yao, X. Q. Wang, Y. Liu and Z. B. Wu, *Appl. Surf. Sci.*, 2019, **467**, 439-445.
8. C. Liu, F. Li, J. Wu, X. Hou, W. Huang, Y. Zhang and X. G. Yang, *J. Hazard. Mater.*, 2019, **363**, 439-446.
9. L. Cao, X. D. Wu, Y. F. Xu, Q. W. Lin, J. F. Hu, Y. Chen, R. Ran and D. Weng, *Catal. Commun.*, 2019, **120**, 55-58.
10. Z. Y. Sheng, Y. F. Hu, J. M. Xue, X. M. Wang and W. P. Liao, *J. Rare Earth.*, 2012, **30**, 676-682.
11. C. Niu, X. Y. Shi, K. Liu, Y. You, S. X. Wang and H. He, *Catal. Commun.*, 2016, **81**, 20-23.
12. S. Han, J. Cheng, Q. Ye, S. Y. Cheng, T. F. Kang and H. X. Dai, *Micropor. Mesopor. Mat.*, 2019, **276**, 133-146.
13. H. Liu, Z. X. Fan, C. Z. Sun, S. H. Yu, S. Feng, W. Chen, D. Z. Chen, C. J. Tang, F. Gao and L. Dong, *Appl. Catal. B-Environ.*, 2019, **244**, 671-683.
14. L. Q. Chen, F. L. Yuan, Z. B. Li, X. Y. Niu and Y. J. Zhu, *Chem. Eng. J.*, 2018, **354**, 393-406.
15. T. R. Zhang, S. B. Ma, L. Q. Chen, R. Li, X. S. Leng, Y. S. Li, F. L. Yuan, X. Y. Niu and Y. J. Zhu, *Appl. Catal. a-Gen.*, 2019, **570**, 251-261.
16. Z. Y. Fei, Y. R. Yang, M. H. Wang, Z. L. Tao, Q. Liu, X. Chen, M. F. Cui, Z. X. Zhang, J. H. Tang and X. Qiao, *Chem. Eng. J.*, 2018, **353**, 930-939.
17. Y. Jiang, C. Z. Lai, S. J. Liu, G. T. Liang, C. Z. Bao, W. Y. Shi and S. Y. Ma, *Aerosol Air Qual. Res.*, 2019, **19**, 422-430.
18. F. Y. Gao, X. L. Tang, H. H. Yi, J. Y. Li, S. Z. Zhao, J. G. Wang, C. Chu and C. L. Li, *Chem. Eng. J.*, 2017, **317**, 20-31.
19. H. Z. Chang, J. H. Li, X. Y. Chen, L. Ma, S. J. Yang, J. W. Schwank and J. M. Hao, *Catal. Commun.*, 2012, **27**, 54-57.
20. H. Z. Chang, X. Y. Chen, J. H. Li, L. Ma, C. Z. Wang, C. X. Liu, J. W. Schwank and J. M. Hao, *Environ. Sci. & Technol.*, 2013, **47**, 5294-5301.
21. X. S. Leng, Z. P. Zhang, Y. S. Li, T. R. Zhang, S. B. Ma, F. L. Yuan, X. Y. Niu and Y. J. Zhu, *Fuel Process. Technol.*, 2018, **181**, 33-43.
22. K. Yang, H. Yi, X. Tang, S. Z. Zhao, F. Y. Gao, Y. H. Huang, Z. Y. Yang, J. G. Wang, Y. R. Shi and X. Z. Xie, *Chem. Eng. J.*, 2019, **364**, 420-427.
23. Z. Y. Sheng, D. R. Ma, D. Q. Yu, X. Xiao, B. J. Huang, L. Yang and S. Wang, *Chinese J. Catal.*, 2018, **39**, 821-830.
24. L. Chen, X. X. Wang, Q. L. Cong, H. Y. Ma, S. J. Li and W. Li, *Chem. Eng. J.*, 2019, **369**, 957-967.
25. L. P. Han, M. Gao, J. Y. Hasegawa, S. X. Li, Y. J. Shen, H. R. Li, L. Y. Shi and D. S. Zhang, *Environ. Science & Technology*, 2019, **53**, 6462-6473.
26. W. Li, J. P. Yang, Z. X. Wu, J. X. Wang, B. Li, S. S. Feng, Y. H. Deng, F. Zhang and D. Y. Zhao, *J. Am. Chem. Soc.*, 2012, **134**, 11864-11867.
27. Q. Li, X. Li, W. Li, L. Zhong, C. Zhang, Q. Y. Fang and G. Chen, *Chem. Eng.*

J., 2019, **369**, 26-34.

28. C. Wang, F. Yu, M. Y. Zhu, C. J. Tang, K. Zhang, D. Zhao, L. Dong and B. Dai, *J. Environ. Sci.*, 2019, **75**, 124-135.
29. Y. M. Abbas, A. B. Mansour, S. E. Ali and A. H. Ibrahim, *J. Magn. and Magn. Mater.*, 2019, **482**, 66-74.
30. D. Salinas, P. Araya and S. Guerrero, *Appl. Catal. B-Environ.*, 2012, **117**, 260-267.
31. W. Zhao, S. P. Dou, K. Zhang, L. C. Wu, Q. Wang, D. H. Shang and Q. Zhong, *Chem. Eng. J.*, 2019, **364**, 401-409.
32. X. J. Yao, L. Chen, J. Cao, Y. Chen, M. Tian, F. M. Yang, J. F. Sun, C. J. Tang and L. Dong, *Chem. Eng. J.*, 2019, **369**, 46-56.
33. Y. J. Xie, Y. Y. Yu, X. Q. Gong, Y. Guo, Y. L. Guo, Y. Q. Wang and G. Z. Lu, *Crystengcomm*, 2015, **17**, 3005-3014.
34. S. B. Ma, X. Y. Zhao, Y. S. Li, T. R. Zhang, F. L. Yuan, X. Y. Niu and Y. J. Zhu, *Appl. Catal. B-Environ.*, 2019, **248**, 226-238.
35. M. Kong, Q. C. Liu, L. J. Jiang, W. Tong, J. Yang, S. Ren, J. L. Li and Y. M. Tian, *Chem. Eng. J.*, 2019, **370**, 518-526.
36. A. J. Xie, Y. R. Tang, X. Y. Huang, X. Jin, P. F. Gu, S. P. Luo, C. Yao and X. Z. Li, *Chem. Eng. J.*, 2019, **370**, 897-905.
37. C. L. Li, X. L. Tang, H. H. Yi, L. F. Wang, X. X. Cui, C. Chu, J. Y. Li, R. C. Zhang and Q. J. Yu, *Appl. Surf. Sci.*, 2018, **428**, 924-932.
38. F. X. Li, J. L. Xie, K. Qi, P. J. Gong and F. He, *Catal. Lett.*, 2019, **149**, 788-797.
39. A. Y. Zhou, D. Q. Yu, L. Yang and Z. Y. Sheng, *Appl. Surf. Sci.*, 2016, **378**, 167-173.
40. X. Y. Wang, K. Zhang, W. T. Zhao, Y. Y. Zhang, Z. X. Lang, T. H. Zhang, Y. H. Xiao, Y. F. Zhang, H. Z. Chang and L. L. Jiang, *Ind. & Eng. Chem. Res.*, 2017, **56**, 14980-14994.
41. D. Dogu, K. E. Meyer, A. Fuller, S. Gunduz, D. J. Deka, N. Kramer, A. C. Co and U. S. Ozkan, *Appl. Catal. B-Environ.*, 2018, **227**, 90-101.
42. Y. Geng, X. L. Chen, S. J. Yang, F. D. Liu and W. P. Shan, *Acs Appl. Mater. & Inter.*, 2017, **9**, 16952-16959.
43. T. Lee and H. Bai, *Ind. & Eng. Chem. Res.*, 2018, **57**, 4848-4858.
44. Y. Wang, H. H. Li, S. K. Wang, X. Wang, Z. He and J. J. Hu, *Fuel Process. Technol.*, 2019, **188**, 179-189.
45. L. Chen, X. J. Yao, J. Cao, F. M. Yang, C. J. Tang and L. Dong, *Appl. Surf. Sci.*, 2019, **476**, 283-292.
46. A. J. Xie, Y. Y. Tao, X. Jin, P. F. Gu, X. Y. Huang, X. M. Zhou, S. P. Luo, C. Yao and X. Z. Li, *New J. Chem.*, 2019, **43**, 2490-2500.
47. S. J. Yang, C. X. Liu, H. Z. Chang, L. Ma, Z. Qu, N. Q. Yan, C. Z. Wang and J. H. Li, *Ind. & Eng. Chem. Res.*, 2013, **52**, 5601-5610.
48. B. H. Zhao, R. Ran, X. G. Guo, L. Cao, T. F. Xu, Z. Chen, X. D. Wu, Z. C. Si and D. Weng, *Appl. Catal. a-Gen.*, 2017, **545**, 64-71.
49. J. X. Liu, J. Liu, Z. Zhao, J. B. Tan, Y. C. Wei and W. Y. Song, *Aiche J.*, 2018,

64, 3967-3978.

50. S. X. Cai, D. S. Zhang, L. Y. Shi, J. Xu, L. Zhang, L. Huang, H. R. Li and J. P. Zhang, *Nanoscale*, 2014, **6**, 7346-7353.
51. L. J. Jiang, Q. C. Liu, G. J. Ran, M. Kong, S. Ren, J. Yang and J. L. Li, *Chem. Eng. J.*, 2019, **370**, 810-821.
52. L. Gao, C. T. Li, S. H. Li, W. Zhang, X. Y. Du, L. Huang, Y. C. Zhu, Y. B. Zhai and G. M. Zeng, *Chem. Eng. J.*, 2019, **371**, 781-795.

View Article Online
DOI: 10.1039/C9NJ03461G

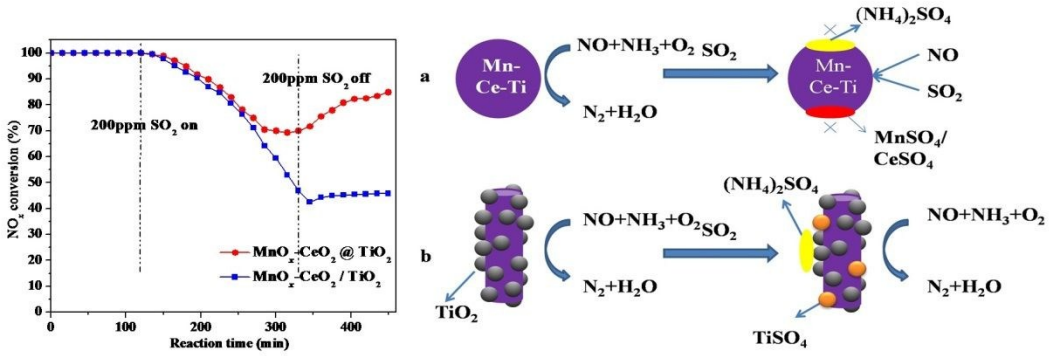

MnO_x-CeO_2 @ TiO_2 catalyst presents excellent NH_3-SCR activity and TiO_2 shell is responsible for the good SO_2 tolerance.